Field-induced double dome and Bose-Einstein condensation in the crossing quantum spin chain system $AgVOAsO_4$

Franziska Weickert,[1,*] Adam A. Aczel,[2,†] Matthew B. Stone,[2] V. Ovidiu Garlea,[2] Chao Dong,[3] Yoshimitsu Kohama,[3] Roman Movshovich,[4] Albin Demuer,[5] Neil Harrison,[6] Monika B. Gamża,[7,8] Alexander Steppke,[7] Manuel Brando,[7] Helge Rosner,[7] and Alexander A. Tsirlin[7,9]

[1]*NHMFL, Florida State University, Tallahassee, Florida 32310, USA*
[2]*Neutron Scattering Division, Oak Ridge National Laboratory, Oak Ridge, Tennessee 37831, USA*
[3]*ISSP, International MegaGauss Science Laboratory, University of Tokyo, Kashiwa, Chiba 277-8581, Japan*
[4]*MPA-CMMS, Los Alamos National Laboratory, Los Alamos, New Mexico 87545, USA*
[5]*GHMFL, Centre National de la Recherche Scientifique, 38042 Grenoble Cedex 9, France*
[6]*MPA-Mag, Los Alamos National Laboratory, Los Alamos, New Mexico 87545, USA*
[7]*MPI CPfS, Nöthnitzer Strasse 40, 01187 Dresden, Germany*
[8]*Jeremiah Horrocks Institute for Mathematics, Physics, and Astrophysics, University of Central Lancashire, PR1 2HE, Preston, United Kingdom*
[9]*Experimental Physics VI, Center for Electronic Correlations and Magnetism, University of Augsburg, 86135 Augsburg, Germany*

(Received 14 February 2019; revised manuscript received 7 June 2019; published 17 September 2019)

We present inelastic neutron-scattering data on the quantum paramagnet $AgVOAsO_4$ that establish this system as a $S = 1/2$ alternating spin chain compound and provide a direct measurement of the spin gap $\Delta = 1.2$ meV. We also present experimental evidence for two different types of field-induced magnetic order between $\mu_0 H_{c1} = 8.4$ T and $\mu_0 H_{c2} = 48.9$ T, which may be related to Bose-Einstein condensation (BEC) of triplons. Thermodynamic measurements in magnetic fields up to 60 T and temperatures down to 0.1 K reveal a $H - T$ phase diagram consisting of a dome encapsulating two ordered phases with maximum ordering temperatures of 3.8 and 5.3 K, respectively. This complex phase diagram is not expected for a single-$\vec{Q}$ BEC system and therefore establishes $AgVOAsO_4$ as a promising multi-$\vec{Q}$ BEC candidate capable of hosting exotic vortex phases.

DOI: 10.1103/PhysRevB.100.104422

I. INTRODUCTION

Magnetic vortices are topological objects expected by theory [1] to occur in quantum magnets with spin-gapped ground states and field-induced XY-antiferromagnetic (AFM) order with a z-axis spin modulation that can be described within the formalism of Bose-Einstein condensation (BEC). Their close similarities to magnetic skyrmions make them highly attractive for technological applications, e.g., because skyrmions are discussed as energetically robust basic units for memory storage. Whereas magnetic skyrmions have been observed experimentally in metallic MnSi [2] and insulating Cu_2OSeO_3 [3] gathering significant scientific attention in recent years, the observation of magnetic vortices in quantum paramagnets has been elusive so far. A necessary condition for the observation of magnetic vortices is the emergence of a multi-$\vec{Q}$ BEC. Here, linear combinations of multiple ordering vectors $\vec{Q}$ can lead to incommensurate AFM order in adjacent phases under the application of a magnetic field, in contrast to single-$\vec{Q}$ BEC, where only one commensurate XY-AFM phase is observed.

Single-$\vec{Q}$ BEC materials often consist of interacting dimers of spin-1/2 ions. The nonmagnetic $S = 0$ singlet ground state is separated from the excited $S = 1$ triplet states by a spin gap, Δ, with a finite dispersion for the triplet excitation arising from the interdimer exchange interactions [4–13]. An applied magnetic field, H, splits the triplet into its three branches according to their S^z quantum number. As the magnetic field increases, the spin gap closes at a critical field, H_{c1}, and generates field-induced magnetic order. If $O(2)$ rotational invariance is preserved above H_{c1}, then this ordered state is equivalent to a BEC of $S^z = 1$ triplons [14–18]. At higher fields, a saturated magnetic phase is generated above H_{c2}. The main difference between single-$\vec{Q}$ and multi-$\vec{Q}$ BEC materials are competing interdimer exchange interactions only present in the latter case. Frustration modifies the triplet dispersion of a multi-$\vec{Q}$ BEC material in a way that several degenerate minima occur inside a single Brillouin zone (BZ), whereas only one exists at the BZ border in the single-$\vec{Q}$ case.

One promising material recently discussed in the context of multi-$\vec{Q}$ BEC is $Ba_3Mn_2O_8$. Inelastic neutron-scattering (INS) measurements [19,20] report evidence for frustrated interdimer exchange and a triplet dispersion consisting of several energy minima in a single Brillouin zone. Intriguingly, thermodynamic and torque magnetometry measurements determined that the H-T phase diagram was more complex than expected for a single-$\vec{Q}$ BEC system, with two ordered phases I and II found for all field orientations except $\vec{H} \| c$ where only one ordered phase was uncovered [9,21]. Subsequent neutron-diffraction measurements in a horizontal scattering plane with an applied field $\vec{H} \| a^*$ identified phases I and II as

*weickert@lanl.gov
†aczelaa@ornl.gov

an incommensurate spin spiral and spin-density wave states, respectively [22], but nuclear magnetic resonance (NMR) work argued that the BEC description only holds for $\vec{H} \| c$ [23]. Other material candidates are therefore required, if one hopes to identify exotic multi-$\vec{Q}$ BEC states, including the magnetic vortex crystal, in the laboratory.

To this end, we propose $AgVOAsO_4$ as a $S = 1/2$ compound to be a promising multi-$\vec{Q}$ BEC candidate. Vanadium V^{4+} is a magnetically isotropic ion with small spin-orbit coupling favoring magnetically ordered ground states of high spin symmetry as represented by BEC. The monoclinic crystal structure of $AgVOAsO_4$ consists of corner-sharing VO_6 octahedra that form structural chains along the crystallographic c direction; these chains are linked to one another via AsO_4 tetrahedra to form a three-dimensional network. The crystal structure is shown in Fig. 1 with panel (a) illustrating the crystal structure viewed roughly along the c axis. There are chain structures along this axis with a V-V distance of 3.639 Å at T = 20 K. In Fig. 1(b) we reproduce the proposed spin model [24] showing only the V sites. We note that the J_a and J_c exchange connect spins between layers. In Figures 1(c) and 1(d) we show views along the (110) and (1$\bar{1}$0) direction. There are two types of structural chains along these directions, which are arranged nearly orthogonal to each other. We label these two chains as type i and type ii. The two chains have very similar vectors and distances between V sites, but their bonding is quite different. The type-i chain structure has a much more planar configuration of coordinated oxygen atoms than the type-ii chain as shown in the middle layer of chains in Fig. 1(c). When viewed along the (1$\bar{1}$0) direction, it is the top and bottom layers of chains [Fig. 1(d)] that have a more planar oxygen coordination. The type-i chain, shown in Fig. 1(e), has been considered to be the magnetic alternating spin chain based upon density functional theory (DFT) calculations [24] with d_i being the dimer bond, J, whereas d_i' is the distance of the interdimer interaction, J'. The dimer-dimer vector is $u_0 = d_i + d_i'$, which corresponds to the (110) and (1$\bar{1}$0) directions depending upon which ab plane the chain resides within. The V-V vectors at 20 K are $d_i = [0.488, -0.525, 0.060]$ and $[0.488, 0.525, 0.060]$ ($|d_i| = 5.59$ Å), $d_i' = [0.512, -0.475, -0.060]$ and $[0.512, 0.475, -0.060]$ ($|d_i'| = 5.56$ Å), $d_{ii} = [0.512, 0.525, -0.060]$ and $[-0.512, 0.525, 0.060]$ ($|d_{ii}'| = 5.90$ Å), and $d_{ii}' = [0.488, 0.475, 0.060]$ and $[-0.488, 0.475, -0.060]$ ($|d_{ii}'| = 5.23$ Å).

Bulk characterization and ^{75}As NMR measurements suggest that $AgVOAsO_4$ is a quantum paramagnet based on alternating spin chains [25–27] with a spin gap $\Delta = 1.1$ meV, $\mu_0 H_{c1} = 10$ T, a saturation field $\mu_0 H_{c2} = 48.5$ T, and an intrachain exchange ratio $\alpha = J'/J \simeq 0.6$–0.7 [24,28]. DFT calculations furthermore predict significant, competing interchain exchange interactions leading to a large degree of magnetic frustration, which may produce the complicated triplet dispersion that is a prerequisite for a multi-$\vec{Q}$ BEC. The relatively small spin gap ensures that these field-induced ordered states are accessible in the laboratory. In this paper, we first show INS results on polycrystalline $AgVOAsO_4$ that establish the alternating spin chain model [24] and provide a direct measurement of the spin gap. Second, we present a comprehensive study of the field-induced magnetic order in this material. Our combined specific-heat, magnetization, and magnetocaloric effect (MCE) measurements on polycrystalline samples establish a complex $H - T$ phase diagram with two different field-induced ordered states, which is not expected

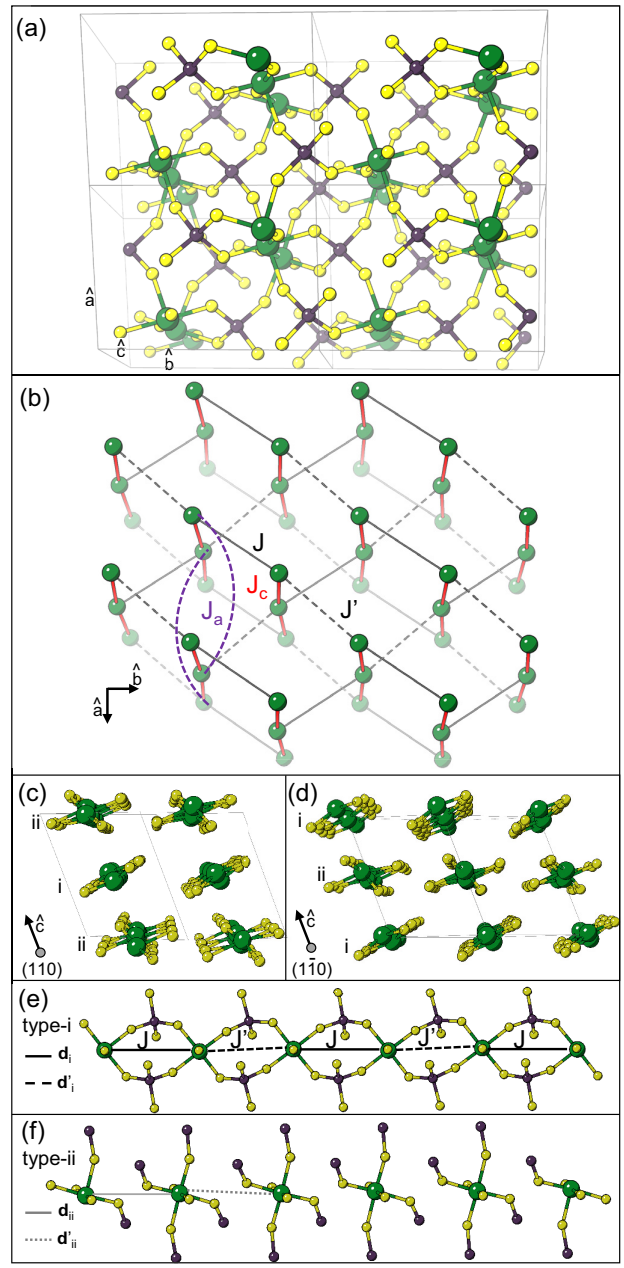

FIG. 1. Crystal structure of $AgVOAsO_4$. V atoms are large green spheres, O atoms are small yellow spheres, and As atoms are black spheres. The Ag atoms are not shown for clarity. (a) Crystal structure viewed obliquely along the c axis. (b) Exchange paths viewed roughly along the c axis. For clarity, the J_a interaction is shown only for a single ac plane and only the V sites are shown. (c) The crystal structure viewed along the (110) direction. (d) The crystal structure viewed along the (1$\bar{1}$0) direction. In (c) and (d), chains of type i and type ii are labeled accordingly. (e) Type-i structural chain with exchange interactions J and J' labeled for vectors d_i and d_i', respectively. (f) Type-ii structural chain with vectors d_{ii} and d_{ii}' shown.

for a single-$\vec{Q}$ BEC system. Therefore, $AgVOAsO_4$ is a strong candidate for hosting multi-$\vec{Q}$ BEC.

II. EXPERIMENTAL RESULTS

A. Neutron-scattering experiments

The synthesis of polycrystalline samples is described elsewhere [24]. INS data were collected on 10 g of $AgVOAsO_4$ using the hybrid spectrometer (HYSPEC) of the Spallation Neutron Source, Oak Ridge National Laboratory. All data were obtained using incident energies of $E_i = 7.5$ or 15 meV, with corresponding Fermi chopper frequencies of 180 and 300 Hz, resulting in instrumental energy resolutions of 0.3 and 0.7 meV Gaussian full width at half maximum, respectively, at the elastic line. The HYSPEC instrument is able to extend the range of measured wave-vector transfer, Q, at a fixed incident energy by moving its detector bank to larger scattering angles. This was done for both the $E_i = 7.5$ and 15 meV measurements presented here. A liquid He cryostat was used during the measurements to achieve temperatures between 3.2 and 200 K.

Figures 2(a) and 2(b) show INS data collected at the HYSPEC instrument with energy resolution $E_i = 7.5$ meV at $T = 50$ and 3.2 K, respectively. At 3.2 K, we observe a band of scattering between 1.5 and 5 meV energy transfer, $\hbar\omega$, with intensity that decreases rapidly as a function of the wave-vector transfer, Q. The intensity of this excitation displays a distinct, oscillatory Q dependence. Both, the temperature and wave-vector dependence of this mode are hallmarks of magnetic fluctuations arising from excited triplet states in a dimerized magnet. No magnetic excitations of higher energy are observed, when neutrons of $E_i = 15$ meV incident energy are used to obtain the data (not shown).

With the magnetic origin of the spectrum established, we next performed an analysis of the INS data using the powder-averaged first frequency moment $\langle E(Q)\rangle$ approach. More specifically, we turn to the following equation, valid for an isotropic spin system with Heisenberg exchange interactions [20,29,30]:

$$\langle E(Q)\rangle \propto -\Sigma J_j \langle S_0 \cdot S_{d_j}\rangle |f(Q)|^2 \left(1 - \frac{\sin Qd_j}{Qd_j}\right) \quad (1)$$

where $f(Q)$ is the magnetic form factor for V^{4+}, J_j is the exchange interaction between magnetic ions with spin S separated by a distance d_j, and $\langle S_0 \cdot S_{d_j}\rangle$ is the two-spin correlation function for this pair. The integration ranges used to extract the first frequency moment from the $E_i = 7.5$ and 15 meV measurements were set to 1.5–5 and 1.25–5 meV, respectively, and the data are shown in Fig. 3. Both measurements have an oscillatory intensity that decreases as Q increases. The two datasets were simultaneously fit to Eq. (1) considering only a single value $d_j = d$, but with a multiplicative prefactor and a constant background unique to each value of incident energy. The results of this comparison are shown as solid curves in Fig. 4 revealing excellent agreement for a distance $d = 5.63(4)$ Å. This value is closer to and within error of the type-i chain distance compared to the type-ii chain intradimer distance. If we fix the value of d in the comparison, we find that the reduced χ^2 value is less for the type-i chain distance

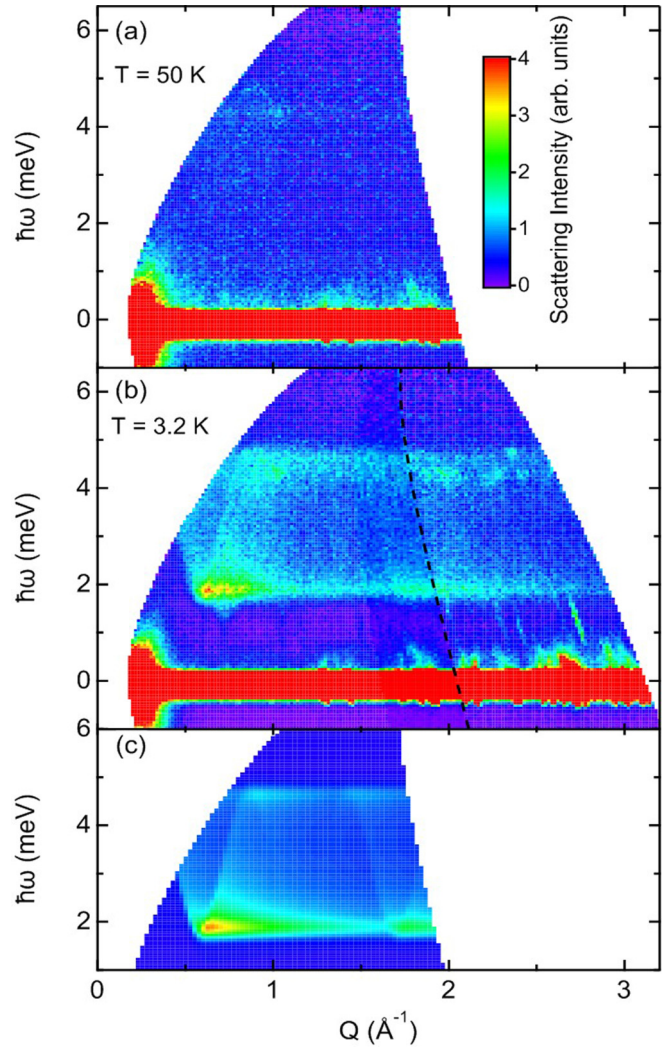

FIG. 2. (a), (b) Color contour plots of the $E_i = 7.5$-meV HYSPEC data for $AgVOAsO_4$ at $T = 50$ and 3.2 K. A gapped magnetic excitation spectrum is clearly visible in the low-temperature data. The data to the left of the black dashed line in (b) were collected using a single orientation for the HYSPEC detector bank. (c) Color contour plot for the alternating chain model described in the text with best-fit parameters $J = 3.43(7)$ meV and $J' = 2.25(9)$ meV. The INS data were only fit over the Q-$\hbar\omega$ region presented in this figure.

($\chi^2 = 6.675$) compared to the value for the type-ii chain distance ($\chi^2 = 8.602$). We therefore conclude that magnetic coupling is mediated only along structural chain i and not along ii.

Our INS results agree well with a previous theoretical study assigning the alternating spin chain model based on band-structure calculations [24] to $AgVOAsO_4$ with leading J and J' along the structural chain i in the crystal structure. We wish to emphasize that, despite their different directions, the alternating spin chains in $AgVOAsO_4$ feature the same exchange couplings and the same spin gap. This is different from the ambient-pressure polymorph of $(VO)_2P_2O_7$ [31], where two distinct spin gaps arise from two types of spin chains with dissimilar exchange couplings.

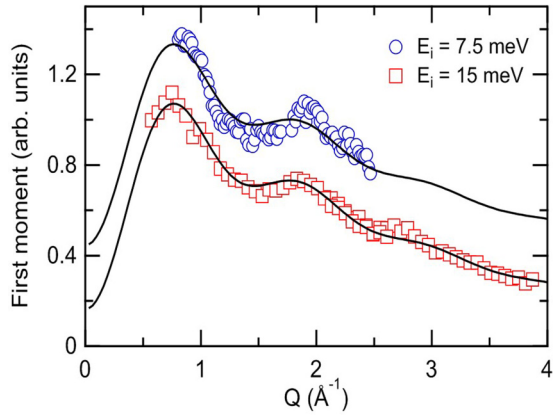

FIG. 3. The powder-averaged first frequency moment as a function of wave-vector transfer for both incident energies used in the HYSPEC measurement. An overall normalization factor has been applied so the two datasets can be plotted with the same y axis. The solid curves represent a simultaneous fit of the data to the first frequency moment expression described in the text with a single exchange interaction.

We proceeded to calculate the dynamical structure factor $S(Q,\omega)$ for $AgVOAsO_4$ using the expression for the alternating Heisenberg spin chain model:

$$S(\vec{Q},\omega) = A|f(Q)|^2[1-\cos(\vec{Q}\cdot\vec{d})]\delta[\hbar\omega - \hbar\omega(\vec{Q})] \quad (2)$$

where A is a multiplicative prefactor and $\vec{d}$ is the vector between spins of the dimer pair with distance d_i. The first-order approximation to the alternating chain model dispersion $\hbar\omega(\vec{Q})$ is given by

$$\hbar\omega(\vec{Q}) = J - \frac{J'}{2}\cos(\vec{Q}\cdot\vec{u}_0) \quad (3)$$

where J and J' are the exchange interactions of the alternating chain and $\vec{u}_0$ is the vector connecting the centers of two adjacent dimers. Prior bulk characterization measurements have established that $\alpha = J'/J \approx 0.65$ for $AgVOAsO_4$. This larger value of α places the potential dispersion for $AgVOAsO_4$ far from the first-order approximation for the alternating chain

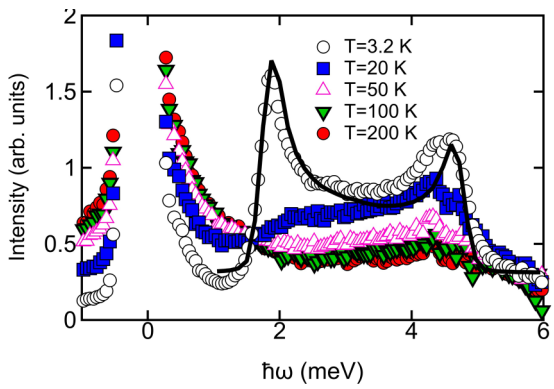

FIG. 4. Temperature dependence of a constant-Q cut with an integration range $Q = [0.35,\ 2]$ Å^{-1} from the $E_i = 7.5$ meV HYSPEC dataset. The solid curve superimposed on the 3.2 K data represents a constant-Q cut taken from the best-fit simulation shown in Fig. 2(c).

model, so we used a modified version of Eq. (3) in our modeling with terms up to third order in α as described in [32,33]. To facilitate a direct comparison with our INS data, we powder-averaged Eq. (2) according to the following:

$$S(Q,\omega) = \int \frac{d\Omega_Q}{4\pi} S(\vec{Q},\omega). \quad (4)$$

More specifically, we calculate $S(\vec{Q},\omega)$ over spherical shells in Q space at fixed values of energy transfer with $\vec{d}$ and $\vec{u}_0$ set to the 20 K crystal structure values [24] for the proposed magnetic type-i alternating chains. We account for the different chain directions in adjacent ab planes by including equal contributions from both crystallographic $[1\bar{1}0]$ and $[110]$ directions in our model. The modified spectrum was then multiplied by the appropriate magnetic form factor, $|f(Q)|^2$, for the vanadium ions and convolved with a Gaussian approximation for the instrumental energy and wave-vector resolution. A constant background and the multiplicative prefactor were incorporated as fitting parameters of the calculated spectrum in comparison to the measured data. This modeling can accurately reproduce the wave-vector and energy dependence of the measurement when $J = 3.43(7)$ meV [39.8(7) K] and $J' = 2.25(9)$ meV [26.2(1) K], as shown in Fig. 2(c). The determined exchange interactions and their ratio $\alpha = J'/J = 0.66(3)$ are in excellent agreement with values determined in previous work [24,28].

Figure 4 shows constant-Q cuts (integration range $Q = [0.35, 2]$ Å^{-1}) for the $E_i = 7.5$ meV data at different temperatures. We superimpose a cut through our model in the figure and find a good overall agreement with the data; however, the measured scattering intensity is not fully captured near the top of the band between 3 and 5 meV. A large portion of this extra intensity persists up to high temperatures. These combined findings are consistent with a small phonon contribution to the measured spectrum that we do not account for in our modeling. On the other hand, this excess scattering may also arise from two-triplon excitations. This scenario is particularly plausible for quantum paramagnets like $AgVOAsO_4$ where the triplet excitation bandwidth is much larger than the spin gap, as the continuum of two-triplon modes will then extend down into the single-particle regime [34] that we have modeled above. Single-crystal INS data will ultimately be required to definitively establish the origin of the additional scattering in the magnetic excitation spectrum of $AgVOAsO_4$.

B. Specific heat

With the alternating chain character confirmed by INS measurements, we now examine the magnetic field and temperature-dependent phase diagram of $AgVOAsO_4$. The small spin gap should be closed at an experimentally accessible critical field H_{c1} and this allows one to search for field-induced magnetic order. We performed specific-heat $C(T)$ measurements using a standard relaxation technique in a Quantum Design physical property measurement system with magnetic fields up to 14 T. The upper inset in Fig. 5 shows the specific heat divided by temperature $C(T)/T$ in zero field, with a broad hump occurring at 13 K as expected for an interacting, alternating spin chain system with a nonmagnetic singlet ground state. We put considerable effort into the

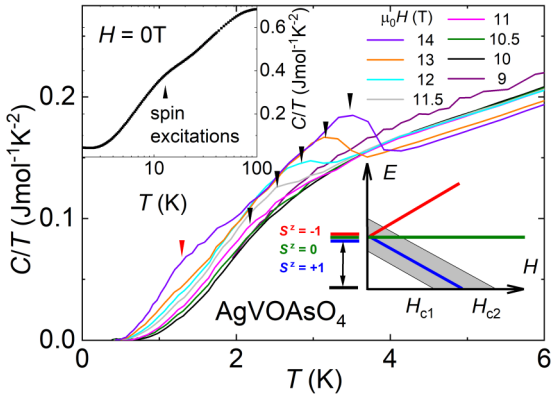

FIG. 5. Specific heat divided by temperature $C(T)/T$ vs T for magnetic fields between 9 and 14 T with nuclear Schottky contributions subtracted. The measurement at 11 T is the first curve that develops a broad maximum at ∼2.2 K that becomes more pronounced and shifts to higher T in stronger fields (marked with black arrows). Additionally, a second anomaly appears at ∼1 K in the 14-T measurement, as indicated by the red arrow. The upper inset shows $C(T)/T$ in zero magnetic field, with a broad hump around 13 K arising from the thermal population of the triplet state. The lower inset displays the energy-level scheme for a spin dimer system with both intradimer and interdimer exchange coupling under the application of an external magnetic field.

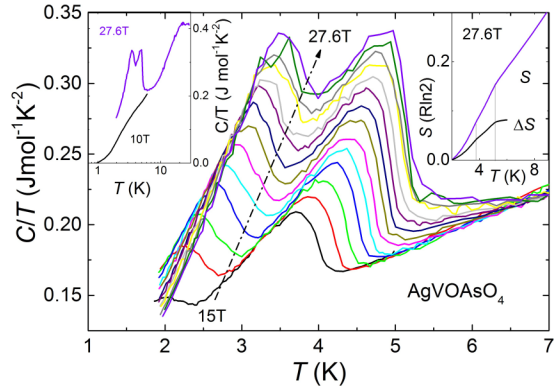

FIG. 6. Specific heat divided by temperature $C(T)/T$ vs T for magnetic fields between 15 and 27.6 T. Two distinct maxima are observed that move to higher temperatures with increasing field and represent clear evidence for multiple field-induced phase transitions below the onset of the saturated paramagnetic phase at H_{c2}. The left inset displays $C(T)/T$ for the 10 T and maximum field 27.6 T measurements. The right inset shows the calculated entropy $S = \int C(T)/T\,dT$ in units R ln 2 for the 27.6 T measurement with (i.e., ΔS) and without (i.e., S) subtraction of the 10 T $C(T)/T$ data.

preparation of a nonmagnetic reference compound to subtract the phonon contribution; however, the nonmagnetic analog $AgTiOAsO_4$ does not exist or at least cannot be synthesized under standard conditions.

The specific heat divided by temperature $C(T)/T$ versus T for magnetic fields between 9 and 14 T, with appropriate nuclear Schottky contributions subtracted (discussion below), is shown in Fig. 5. We observe the onset of a broad maximum at 2.2 K in the 11 T data (indicated by a black arrow), in addition to the hump observed at 13 K. This anomaly becomes more pronounced in magnetic fields $\geqslant$11.5 T and provides the first evidence for field-induced magnetic order in this material. A close look at the data obtained at 14 T reveals that the first maximum has shifted to 3.7 K and a second feature in the data is now visible at 1 K, as indicated by the red arrow in Fig. 5.

To map out a larger region of the $H-T$ phase diagram, we extended our measurements of specific heat to 27.6 T in a resistive magnet at the Laboratoire National des Champs Magnetiques Intenses in Grenoble, France, using a relaxation dual slope technique [35]. The data are shown in Fig. 6. We observe that both maxima in $C(T)/T$ develop into distinct λ anomalies for $H > 15$ T that are typical for second-order phase transitions. Specific heat measurements in high magnetic fields often show a significant nuclear Schottky contribution $[C(T)/T]_{ns}$ at low T caused by isotopes with nonzero nuclear spin. In $AgVOAsO_4$, ^{107}Ag and ^{109}Ag ($I = 1/2$, 50% natural abundance each), ^{51}V (7/2, 99%), and ^{75}As (3/2, 100%) contribute to this effect. We subtract a contribution of the form $[C(T)/T]_{ns} = a_0 T^{-3}$ from the data shown in Fig. 5. The estimated prefactor $a_0 = 1.55$ mJ K/mol in low fields increases by 30% for the 14 T measurement. Enlarged a_0 values above H_{c1} are a further indication for field-induced order, since the internal magnetic field detected by the nuclear spins is strongly enhanced.

The full entropy of a spin-1/2 dimer system is R ln 2, which is released when the thermal energy is significantly larger than the intradimer exchange J [36]. Since our INS measurements find the primary exchange constant to be approximately $J = 40$ K, we expect the high-T entropy regime to onset well above the 13 K maximum observed in the zero-field specific-heat data. In the left inset of Fig. 6, we show $C(T)/T$ for the 10 and 27.6 T measurements on the same scale to facilitate an easier comparison. The right inset shows the calculated entropy for the 27.6 T measurement with (i.e., ΔS) and without (i.e., S) subtraction of the specific heat measured at 10 T. About 30% of the maximum entropy R ln 2 is recovered upon warming up to 10 K with only a few percent released at each of the two phase transitions. As shown later, these small differences in entropy are sufficiently large to track the phase boundaries in MCE measurements under quasiadiabatic conditions.

C. Magnetization

We continue our high-field study with magnetization measurements. Extraction magnetometry has been utilized to measure $M(H)$ between 0.5 and 10 K up to 60 T inside a capacitor-driven pulsed magnet at the Pulsed Field Facility of the National High Magnetic Field Laboratory. Signatures in $M(H)$ have been used successfully in the past to estimate the phase diagram of related compounds [37]. Figure 7 shows the magnetization of $AgVOAsO_4$ measured up to 60 T with the initial sample temperature $T_0(H = 0)$ in the range between 0.56 and 10 K. At low T, we can distinguish three different field regions. In fields up to 5 T, the magnetization is dominated by the paramagnetic behavior of unpaired spins arising from defects in the crystal structure [28]. Above 5 T these unpaired spins are fully polarized, which leads to a

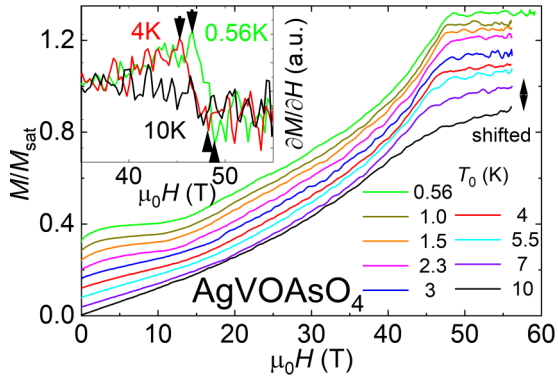

FIG. 7. Magnetization $M(H)$ vs magnetic field H measured in high fields to 60 T shown for initial temperatures T_0 between 0.56 and 10 K (data are offset vertically for better visibility). The inset shows dM/dH close to H_{c2} for the measurements at 0.56 and 4 K with a clear maximum followed by a step down indicating a double phase transition. In contrast, a more smooth behavior in dM/dH is observed at 10 K.

constant background in the quantum paramagnetic state. Starting at a critical field H_{c1} near 10 T, the magnetization increases monotonically and reaches saturation at about 48 T. The field dependence of $M(H)$ can be reproduced with an interacting, alternating spin chain model [24]. The magnetization close to full saturation reveals two distinct changes in the slope at $\mu_0 H_{c2'} = 46.6$ T and $\mu_0 H_{c2} = 48.8$ T, as can be seen more clearly in the derivative $\partial M/\partial H$ in the inset of Fig. 7.

In order to identify multiple phase transitions in magnetization measurements close to the lower critical field H_{c1}, we extend our experiments down to 0.1 K temperature. This approach is necessary because quantum fluctuations significantly alter thermodynamic signatures of second-order phase transitions at the onset of field polarization in quantum magnets. The effect depends on the renormalized mass m^* of the bosons, which scales with the ratio of the critical fields: $m^* \propto H_{c1}/H_{c2}$ at H_{c1} [38]. Notably, mass renormalization does not occur close to H_{c2}, because here the fully polarized system behaves classically. Therefore, asymmetric thermodynamic anomalies (i.e., sharper near H_{c2} versus near H_{c1}) are expected in AgVOAsO$_4$. Figure 8 shows $M(H)$ versus H for magnetic fields between 7.4 and 12 T. A dilution refrigerator equipped with a 12 T superconducting magnet and a Faraday magnetometer was used to obtain $M(H)$ and $M(T)$ down to 0.1 K close to the critical fields H_{c1} and H'_{c1}. We observe two slope changes in $M(H)$, corresponding to two weakly T-dependent phase transitions, at $\mu_0 H_{c1} = 8.4$ T and at $\mu_0 H_{c1'} = 10.5$ T. We also carried out T-dependent $M(T)$ measurements in constant magnetic fields between 7 and 12 T, and we find a very small T dependence in the data as expected from the light boson mass. A maximum in $M(T)$ is observed at the lower $H_{c1}(T)$ phase boundary, as seen in the inset of Fig. 8, that moves to higher T with increasing field, but no clear signature in $M(T)$ is resolved close to the $H_{c1'}(T)$ phase boundary line.

D. Phase diagram and MCE

Figure 9 summarizes the phase transitions obtained by specific-heat and magnetization measurements in pulsed and

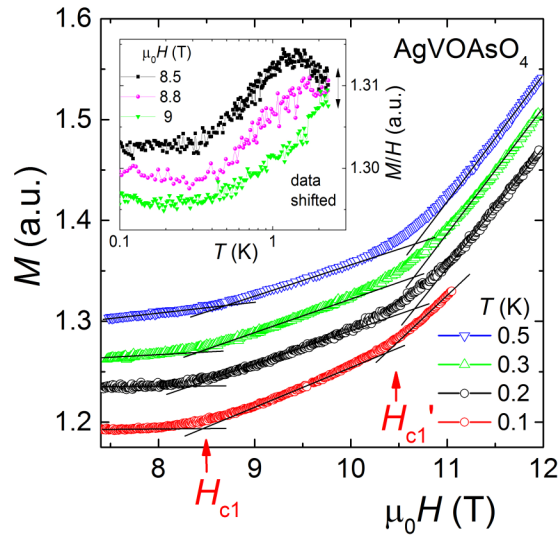

FIG. 8. Magnetization $M(H)$ vs magnetic field H in the field range 7.4 to 12 T for T between 0.1 and 0.5 K. The measurements are offset from one another to ensure better visibility. We observe two changes of slope in $M(H)$ at $\mu_0 H_{c1} = 8.4$ T and $\mu_0 H_{c1'} = 10.5$ T, which identify two field-induced phase transitions. The inset shows $M(T)/H$ vs T collected in fields of 8.5, 8.8, and 9 T. A broad maximum is observed in these data that is used to define the H_{c1} phase boundary.

static magnetic fields. These measurements map out a double-dome phase diagram with $\mu_0 H_{c1} = 8.4$ T, $\mu_0 H_{c1'} = 10.5$ T, $\mu_0 H_{c2'} = 46.6$ T, and $\mu_0 H_{c2} = 48.9$ T. We complete our investigations of the high-field properties in AgVOAsO$_4$ with MCE measurements carried out in a capacitor-driven pulsed

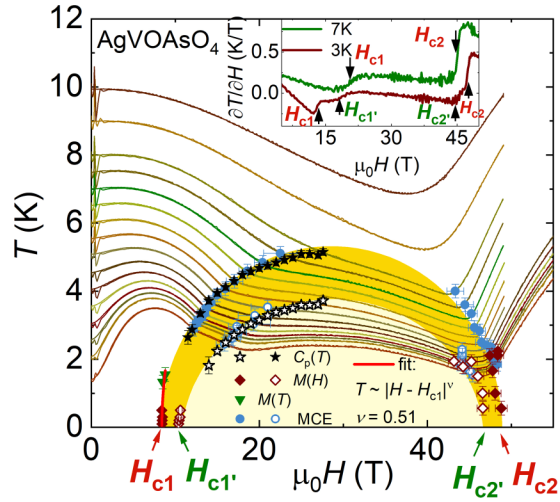

FIG. 9. $H-T$ phase diagram of AgVOAsO$_4$ obtained from specific heat, MCE, and magnetization experiments. We observe clear signatures of two different field-induced ordered states. Lines of constant entropy obtained under adiabatic conditions in pulsed fields illustrate the MCE and confirm the double dome structure of the phase diagram. A power-law fit $T \propto |H - H_{c1}|^{\nu}$ of the phase boundary at H_{c1} reveals 0.51 as the critical exponent. The inset shows the derivative $\partial T/\partial H$ for MCE measurements with zero-field temperatures $T_0 = 3$ and 7 K. Arrows mark the critical fields H_{c1}, $H_{c1'}$, $H_{c2'}$, and H_{c2}.

magnet (pulse duration 36 ms) at the International MegaGauss Science Laboratory of the University of Tokyo. In the experiment, the sample is kept under quasiadiabatic conditions during fast changing field pulses and the sample temperature is monitored, which yields isentropic temperature lines as included in Fig. 9. The polarization of free spins up to 5 T is reflected in a smooth increase of the temperature because the entropy decreases gradually. A careful analysis of the derivative $\partial T/\partial H$, shown for the $T_0 = 3$ and 7 K measurements in the inset of Fig. 9, reveals four clear steps corresponding to the crossing points of the four phase transitions in the 3 K data, whereas only two steps are resolved in the 7 K measurement. These results are consistent with the phase lines extracted from specific-heat and magnetization measurements. Furthermore, the MCE isentropes exhibit a clear asymmetric behavior with a shallow minimum in $T(H)$ close to H_{c1} indicating a (relative) small entropy accumulation and a deeper minimum around H_{c2} indicating more accumulated entropy. This effect can be explained again with a renormalized boson mass close to H_{c1} and a bare boson mass close to H_{c2}. Moreover, the MCE measurements allow us to refine the actual sample temperature in the magnetization experiments when crossing through the phase boundaries, because the magnetization and MCE measurements were collected under similar quasiadiabatic conditions in pulsed magnetic fields.

III. DISCUSSION

We want to emphasize that a clear double anomaly observed in both the low- and high-field regimes of the $H-T$ phase diagram for $AgVOAsO_4$ cannot be explained by magnetic anisotropy. For a polycrystalline, anisotropic sample, only one broad anomaly in $C(T)/T$ is expected because all grains are randomly oriented and therefore should contribute equally to the anomaly through a continuous spectrum of critical fields. Also, we found no evidence for anisotropy-induced splitting of the triplet excitation in our INS measurements. We furthermore can rule out antisymmetric exchange interactions based on symmetry considerations. $AgVOAsO_4$ belongs to the space group $P2_1/c$ that features inversion centers between the vanadium atoms [24]. Finally, electron-spin resonance measurements reveal a nearly isotropic g factor [24], with $g_\parallel = 1.92$ and $g_\perp = 1.96$. The 2% g factor anisotropy is equivalent to a 0.2 T difference in the critical fields $\mu_0|H_{c1} - H_{c1'}|$ and less than a 1 T difference $\mu_0|H_{c2} - H_{c2'}|$. These values are much smaller than the 2 T difference in the critical fields that we have identified here on both the low- and high-field sides of the phase diagram.

Both phase transitions can be classified as second order, because (i) the anomaly in $C(T)/T$ shows the typical λ shape, (ii) no hysteresis or dissipative behavior is observed in the measurements, and (iii) we observe asymmetry in the thermodynamic anomalies measured at H_{c1} and H_{c2}, which are caused by quantum fluctuations only present at second-order transitions. Subsequently, we analyze the critical behavior of the phase boundary up to 1.55 K (Fig. 9) with a power law $T \propto |H - H_{c1}|^\nu$ using $\mu_0 H_{c1} = 8.4$ T and we obtain $\nu = 0.51 \pm 0.13$. This value corroborates the three-dimensional BEC scenario ($\nu = 2/3$) [39].

Theoretical work based on density-matrix renormalization-group calculations for $\alpha = 0.45$ in the alternating chain model finds a complex $H-T$ phase diagram with a phase of incommensurate magnetic order terminated by a first-order transition inside a larger dome of a commensurate one [40–42]. The asymmetric inner dome appears when intrachain next-nearest-neighbor frustration exceeds 10% of nearest-neighbor coupling, which is equivalent to bond frustration connecting the *same dimers in the same chain* [4]. We want to stress that $AgVOAsO_4$ represents the case of frustrated exchange interactions connecting alternating chains and therefore *different dimers* in different *ab* planes [24]. Only for the latter case, a multi-Q BEC is expected with coexistence of XY-AFM and Ising-like ordering in the very same phase [4]. The magnetic isotropy of the V^{4+} moments, the symmetry of the phase diagram, the frustrated interdimer interactions, as well as the second-order phase boundaries found for $AgVOAsO_4$ point to the possibility to find multi-$\vec{Q}$ BEC in this material.

IV. SUMMARY

In summary, we have used inelastic neutron-scattering experiments on polycrystalline samples of the quantum paramagnet $AgVOAsO_4$ to confirm that this system is well described by an alternating spin chain model. We have established the $H-T$ phase diagram for $AgVOAsO_4$ with specific heat, MCE, and magnetization measurements in high magnetic fields and down to low temperatures. We find evidence for a symmetric double-dome phase diagram with field-induced order between $\mu_0 H_{c1} = 8.4$ T and $\mu_0 H_{c2} = 48.9$ T. This complex phase diagram establishes $AgVOAsO_4$ as a promising multi-$\vec{Q}$ BEC candidate capable of hosting exotic topological spin structures. Future NMR or neutron-diffraction measurements on single crystals above the lower critical fields H_{c1} and $H_{c1'}$ are essential for elucidating the microscopic spin arrangements of the two field-induced ordered phases in this material.

ACKNOWLEDGMENTS

F.W. thanks Cristian D. Batista for fruitful discussions. A portion of this research used resources at the Spallation Neutron Source, a DOE Office of Science User Facility operated by Oak Ridge National Laboratory. The National High Magnetic Field Laboratory is supported by the National Science Foundation Cooperative Agreement No. DMR-1157490, the State of Florida, and the United States Department of Energy. N.H. acknowledges support from the following Department of Energy, Basic Energy Science project: Science in 100 Tesla. A.A.T. was supported by the Federal Ministry for Education and Research (Germany) through the Sofja Kovalevskaya Award of Alexander von Humboldt Foundation.

[1] Y. Kamiya and C. D. Batista, Phys. Rev. X **4**, 011023 (2014).

[2] S. Mühlbauer, B. Binz, F. Jonietz, C. Pfleiderer, A. Rosch, A. Neubauer, R. Georgii, and P. Böni, Science **323**, 915 (2009).

[3] S. Seki, X. Z. Yu, S. Ishiwata, and Y. Tokura, Science **336**, 198 (2012).

[4] V. Zapf, M. Jaime, and C. D. Batista, Rev. Mod. Phys. **86**, 563 (2014).

[5] T. Nikuni, M. Oshikawa, A. Oosawa, and H. Tanaka, Phys. Rev. Lett. **84**, 5868 (2000).

[6] M. Jaime, V. F. Correa, N. Harrison, C. D. Batista, N. Kawashima, Y. Kazuma, G. A. Jorge, R. Stern, I. Heinmaa, S. A. Zvyagin, Y. Sasago, and K. Uchinokura, Phys. Rev. Lett. **93**, 087203 (2004).

[7] V. S. Zapf, D. Zocco, B. R. Hansen, M. Jaime, N. Harrison, C. D. Batista, M. Kenzelmann, C. Niedermayer, A. Lacerda, and A. Paduan-Filho, Phys. Rev. Lett. **96**, 077204 (2006).

[8] V. O. Garlea, A. Zheludev, T. Masuda, H. Manaka, L.-P. Regnault, E. Ressouche, B. Grenier, J.-H. Chung, Y. Qiu, K. Habicht, K. Kiefer, and M. Boehm, Phys. Rev. Lett. **98**, 167202 (2007).

[9] E. C. Samulon, Y.-J. Jo, P. Sengupta, C. D. Batista, M. Jaime, L. Balicas, and I. R. Fisher, Phys. Rev. B **77**, 214441 (2008).

[10] A. A. Aczel, Y. Kohama, M. Jaime, K. Ninios, H. B. Chan, L. Balicas, H. A. Dabkowska, and G. M. Luke, Phys. Rev. B **79**, 100409(R) (2009).

[11] A. A. Aczel, Y. Kohama, C. Marcenat, F. Weickert, M. Jaime, O. Ayala-Valenzuela, R. D. McDonald, S. D. Selesnic, H. A. Dabkowska, and G. M. Luke, Phys. Rev. Lett. **103**, 207203 (2009).

[12] H. Yamaguchi, H. Miyagai, M. Yoshida, M. Takigawa, K. Iwase, T. Ono, N. Kase, K. Araki, S. Kittaka, T. Sakakibara, T. Shimokawa, T. Okubo, K. Okunishi, A. Matsuo, and Y. Hosokoshi, Phys. Rev. B **89**, 220402 (2014).

[13] Y. Kono, H. Yamaguchi, Y. Hosokoshi, and T. Sakakibara, Phys. Rev. B **96**, 104439 (2017).

[14] T. Matsubara and H. Matsuda, Prog. Theor. Phys. **16**, 569 (1956).

[15] E. G. Batyev and L. S. Braginskii, Zh. Exp. Tehor. Fiz. **87**, 1361 (1984) [Sov. Phys. JETP **60**, 781 (1984)].

[16] I. Affleck, Phys. Rev. B **43**, 3215 (1991).

[17] T. Giamarchi and A. M. Tsvelik, Phys. Rev. B **59**, 11398 (1999).

[18] T. Giamarchi, C. Rüegg, and O. Tchernyshyov, Nat. Phys. **4**, 198 (2008).

[19] M. B. Stone, M. D. Lumsden, S. Chang, E. C. Samulon, C. D. Batista, and I. R. Fisher, Phys. Rev. Lett. **100**, 237201 (2008).

[20] M. B. Stone, M. D. Lumsden, Y. Qiu, E. C. Samulon, C. D. Batista, and I. R. Fisher, Phys. Rev. B **77**, 134406 (2008).

[21] E. C. Samulon, K. A. Al-Hassanieh, Y.-J. Jo, M. C. Shapiro, L. Balicas, C. D. Batista, and I. R. Fisher, Phys. Rev. B **81**, 104421 (2010).

[22] M. B. Stone, M. D. Lumsden, V. O. Garlea, B. Grenier, E. Ressouche, E. C. Samulon, and I. R. Fisher, Phys. Rev. B **92**, 020415 (2015).

[23] S. Suh, K. A. Al-Hassanieh, E. C. Samulon, I. R. Fisher, S. E. Brown, and C. D. Batista, Phys. Rev. B **84**, 054413 (2011).

[24] A. A. Tsirlin, R. Nath, J. Sichelschmidt, Y. Skourski, C. Geibel, and H. Rosner, Phys. Rev. B **83**, 144412 (2011).

[25] G. Xu, C. Broholm, D. H. Reich, and M. A. Adams, Phys. Rev. Lett. **84**, 4465 (2000).

[26] M. B. Stone, Y. Chen, D. H. Reich, C. Broholm, G. Xu, J. R. D. Copley, and J. C. Cook, Phys. Rev. B **90**, 094419 (2014).

[27] F. Weickert, B. Meier, S. Zherlitsyn, T. Herrmannsdörfer, R. Daou, M. Nicklas, J. Haase, F. Steglich, and J. Wosnitza, Meas. Sci. Technol. **23**, 105001 (2012).

[28] N. Ahmed, P. Khuntia, K. M. Ranjith, H. Rosner, M. Baenitz, A. A. Tsirlin, and R. Nath, Phys. Rev. B **96**, 224423 (2017).

[29] P. C. Hohenberg and W. F. Brinkman, Phys. Rev. B **10**, 128 (1974).

[30] C. Tassel, J. Kang, C. Lee, O. Hernandez, Y. Qiu, W. Paulus, E. Collet, B. Lake, T. Guidi, M.-H. Whangbo, C. Ritter, H. Kageyama, and S.-H. Lee, Phys. Rev. Lett. **105**, 167205 (2010).

[31] T. Yamauchi, Y. Narumi, J. Kikuchi, Y. Ueda, K. Tatani, T. C. Kobayashi, K. Kindo, and K. Motoya, Phys. Rev. Lett. **83**, 3729 (1999).

[32] A. Brooks Harris, Phys. Rev. B **7**, 3166 (1973).

[33] T. Barnes, J. Riera, and D. A. Tennant, Phys. Rev. B **59**, 11384 (1999).

[34] M. B. Stone, I. A. Zaliznyak, T. Hong, C. L. Broholm, and D. H. Reich, Nature (London) **440**, 187 (2006).

[35] S. Riegel and G. Weber, J. Phys. E **19**, 790 (1986).

[36] J. Brambleby, P. A. Goddard, J. Singleton, M. Jaime, T. Lancaster, L. Huang, J. Wosnitza, C. V. Topping, K. E. Carreiro, H. E. Tran, Z. E. Manson, and J. L. Manson, Phys. Rev. B **95**, 024404 (2017).

[37] S. E. Sebastian, N. Harrison, C. Batista, L. Balicas, M. Jaime, P. Sharma, N. Kawashima, and I. Fisher, J. Magn. Magn. Mater. **310**, e460 (2007).

[38] Y. Kohama, A. V. Sologubenko, N. R. Dilley, V. S. Zapf, M. Jaime, J. A. Mydosh, A. Paduan-Filho, K. A. Al-Hassanieh, P. Sengupta, S. Gangadharaiah, A. L. Chernyshev, and C. D. Batista, Phys. Rev. Lett. **106**, 037203 (2011).

[39] F. Weickert *et al.*, Phys. Rev. B **85**, 184408 (2012).

[40] N. Maeshima, K. Okunishi, K. Okamoto, and T. Sakai, Phys. Rev. Lett. **93**, 127203 (2004).

[41] N. Maeshima, K. Okunishi, K. Okamoto, T. Sakai, and K. Yonemitsu, J. Phys. Soc. Jpn. **74**, 63 (2005).

[42] N. Maeshima, K. Okunishi, K. Okamoto, T. Sakai, and K. Yonemitsu, J. Phys.: Condens. Matter **18**, 4819 (2006).